A perturbative approach for efficiently tuning nonempirical hybrid functionals with defect probes

Jing Yang,* Stefano Falletta, and Alfredo Pasquarello

Chaire de Simulation à l'Echelle Atomique (CSEA), Ecole Polytechnique Fédérale de Lausanne (EPFL), CH-1015 Lausanne, Switzerland

E-mail: jing.yang@epfl.ch

Abstract

We present a calculation-efficient procedure for nonempirically tuning hybrid functionals to accurately predict band gaps of solid systems. By inserting an optimized potential probe, we obtain localized electronic state and seek the optimal mixing parameter by enforcing Koopmans' condition on the achieved state. This method yields an averaged band gap error of 0.25 eV for simple *sp* materials and 0.39 eV for 3*d* materials. We further propose a perturbative one-shot approach where the single-particle eigenvalues are calculated with wave functions obtained at the semilocal level, which reduces the computational cost of optimal tuning by an average of 85% without deteriorating the accuracy. Tests on different defect species and functional forms suggest that the scheme is robust in producing accurate band gaps across narrow band-gap and wide band-gap solids.

Kohn-Sham density functional theory (KS-DFT)[1,2] with local-density approximation (LDA) or generalized gradient approximation (GGA) is known to underestimate materials band gap due to the self-interaction error.[3,4] Hybrid functionals open up the gap by

mixing a fraction of the non-local Fock exchange and thus greatly improve the predictions.[5] For instance, the hybrid Perdew-Burke-Ernzerhof (PBE0) functional[6,7] mixes a fraction α = 0.25 of the Fock exchange. Another important group of functionals, commonly named as the range-separated Coulomb attenuating method (CAM)-type functional,[8] separates the nonlocal exchange potential into long-range (LR) and short-range (SR) parts bridged by the error function.

$$\frac{1}{|\mathbf{r}-\mathbf{r}'|} = \underbrace{\frac{1-\mathrm{erf}(\mu|\mathbf{r}-\mathbf{r}'|)}{|\mathbf{r}-\mathbf{r}'|}}_{\mathrm{SR}} + \underbrace{\frac{\mathrm{erf}(\mu|\mathbf{r}-\mathbf{r}'|)}{|\mathbf{r}-\mathbf{r}'|}}_{\mathrm{LR}}. \tag{1}$$

The exchange potential then gives the form

$$v_x(\mathbf{r},\mathbf{r}') = \alpha_s v_x^{\mathrm{sr-Fock}}(\mathbf{r},\mathbf{r}';\mu) + (1-\alpha_s) v_x^{\mathrm{sr-PBE}}(\mathrm{r};\mu) + \alpha_l v_x^{\mathrm{lr-Fock}}(\mathbf{r},\mathbf{r}';\mu) + (1-\alpha_l) v_x^{\mathrm{lr-PBE}}(\mathrm{r};\mu). \tag{2}$$

Here $v_x^{\mathrm{sr-PBE}}(\mathrm{r};\mu)$, $v_x^{\mathrm{lr-PBE}}(\mathrm{r};\mu)$ represent the short-range and long-range semilocal exchange potentials, while $v_x^{\mathrm{Fock}}(\mathbf{r},\mathbf{r}')$ represents the exact Fock exchange. Heyd-Scuseria-Ernzerhof (HSE) is one of the most widely used range-separated functionals, in which μ is set to 0.106 Bohr^{-1}, $\alpha_s = 0.25$, and $\alpha_l = 0$.[9,10] In the limit of $\mu \to 0$, it falls back to the form of PBE0.

Despite the great success of the hybrid functional family in improving band gap description, the parameterized nature of the functionals limits their applicability to specific types of materials. While PBE0 performs well on materials with intermediate band gaps, it overestimates for small band-gap materials in which electrons are easily polarizable and a stronger screening is required, and underestimates for wide band-gap materials in which the screening is minimal.[11] HSE06 functional also suffer from the latter due to the elimination of the long-range Fock exchange.[12] Nonempirical hybrid functionals, for which the mixing parameters are chosen system-specifically satisfying exact constraints, are designed to address this challenge.[11–14] One such direction is to enforce the generalized Koopmans' condition on the system.[15] By creating a localized state in the system where one can add or remove one electron from the orbital and tune the parameters of hybrid functionals to

ensure that the single-particle energy level does not change whether empty or filled, one essentially retains the piecewise linearity of the functional upon electron insertion according to Janak's theory.[16] Enforcing the generalized Koopmans' condition has been demonstrated to be an effective method for determining parameters in hybrid functionals in a nonempirical fashion, yielding accurate description for electronic structures for a wide range of solid-state materials[17–23] as well as molecules.[24–29]

To search for the optimized parameters for the hybrid functionals by enforcing Koopmans' condition, a procedure often times referred to as optimal tuning, requires performing multiple self-consistent hybrid calculations for the localized states. The rather burdensome tuning procedure limits the practical use of Koopmans' method as a cheap alternative to many-body perturbation theory calculations.[30–34] In this paper, we present a calculation-efficient process for applying Koopmans' method on crystalline systems through defect insertion. We simplify the generalized Koopmans' method on two aspects. First, we have shown that by using an adjustable hydrogenic-like potential probe, one can move the defect level within the band gap.[18] The probe is defined by a local potential

$$V_{\mathrm{loc}}(r) = -\frac{1}{r}\mathrm{erf}\left(\frac{r}{\sqrt{2}\sigma}\right), \tag{3}$$

where σ determines the width of the Gaussian charge distribution.The degree of hybridization between the defect state and band states serves as a criterion for selecting the defect that most accurately retains the generalized Koopmans' condition. Second, the defect wave functions obtained by the semilocal approach are oftentimes approximately similar to those obtained through the full self-consistent application of a hybrid functional given that the defect states are properly localized. This allows one to envisage a perturbative approach in which the single-particle energy levels are calculated with semilocal wave functions, avoiding the full self-consistent hybrid calculation and thus greatly reducing the total computational cost. Simplifying and automating the implementation allows us to study systems with larger

number of electrons and semi-core states and test this approach on materials ranging from simple *sp* materials to 3*d* transition metal materials.

All calculations are performed with QUANTUM ESPRESSO[35–37] with plane wave basis sets and normconserving pseudopotentials.[38,39] Semicore states are explicitly included. For the tuning process, 64-atom supercells are used for the defective calculations with Γ-point to obtain the α_K values. Energy cut-offs are individually selected with band gap accuracy within 1 meV. The single-particle defect levels are obtained with no structural relaxation with a convergence criterion of 10^{-8} Ry for each self-consistency step. For charged cell calculations, state-of-the-art finite-size corrections are applied,[40] where ΔE_{corr} is calculated with the Freysoldt-Neugebauer-Van de Walle (FNV) scheme[41] and the correction for the individual KS defect level $\epsilon^{\text{KS}}_{\text{corr}} = -\frac{2}{q}\Delta E_{\text{corr}}$. Unit cells are used for calculating the band gaps with the optimally-tuned α_K using sufficiently dense **k**-point grids which achieve a band gap convergence of 1 meV. The structures of the materials calculated can be found in Ref 42 where experimental lattice parameters are used. Details of optimizing the adjustable potential probe are provided in Section 1 of Supporting Information.

In Figure 1 we demonstrate the tuning procedure for a PBE0(α_K) (K-PBE0) functional with hydrogen interstitial (H) and potential probe (X) states in GaP as an example. For each defect state, we calculate its occupied (D^0) and unoccupied (D^+) single-particle energy level with varying α. These levels evolve linearly with increasing α, and their intersecting point represents the α at which the Koopmans' condition is satisfied. Certain defect types, like the hydrogen interstitial in GaP shown here, hybridize strongly with the band-edge states. In these cases, the defect states are ill-defined and we exclude them from further calculations. We also note that for some of the hybridized states, the single particle level does not change linearly with respect to varying α. An example of Si is given in Figure S2 in Supporting Information where strong non-linearity is observed for the H^+ level and the resulted α_K produces relatively large error. In contrast, tuning the width of the adjustable probe σ moves the defect level close to the middle of the band gap and restore the linear

behavior, as shown by the X^0 and X^+ states in Figure 1. By using the optimized probe, we achieve localized states in all materials considered in this work.

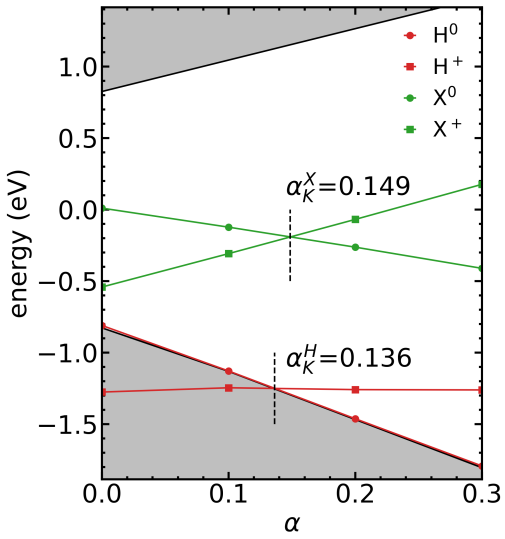

Figure 1: Single-particle energy levels for the probe and hydrogen interstitial defect varying with the mixing parameter α in GaP. The intersecting point of the occupied and unoccupied levels represent α_K which satisfies Koopmans' condition.

Table 1 summarizes the α_K values and corresponding band gaps obtained with the hydrogen interstitial and the optimized probe. Six out of the nineteen materials considered in this work have hydrogen interstitial levels that fall below the valence band. For those materials in which the hydrogen interstitial level fall within the band gap, the resulted α_K by enforcing Koopmans' condition on the hydrogen state does not differ much from the α_K values obtained with the optimized probe. The mean absolute errors (MAEs) in band gap as compared to experimental values are also similar, as shown graphically in Figure 2. This suggests that as long as a well-localized defect state is defined, the Koopmans' scheme is robust in producing similar mixing parameters regardless of the specific defect type. The advantage of using the potential probe is that it provides an automated procedure for locating in-gap defect states that is universally applicable to different materials.

We benchmark the band gaps produced by the K-PBE0 functional in Table 1 by com-

paring with experimental values. Since electron-phonon coupling is not included in the calculations, the zero-point renormalization (ZPR) terms are added to the experimental band gaps to correct for the gap modification due to zero-point motion.[43] For simple *sp* materials, K-PBE0 obtained with the optimized potential probe results in a MAE of 0.27 eV, with a maximal error of 0.69 eV for CaO (band gap 7.09 eV). The prediction accuracy is consistent from narrow band gap materials (1.23 eV for Si) to wide band gap insulators (15.35 eV for LiF) with a mean absolute relative error of 5.1%. However, when 3*d* semi-core states are involved, the K-PBE0 functional appears to systematically underestimate the band gaps. The MAE increases from 0.27 eV to 0.39 eV, with a mean absolute relative error (MARE) of 16.6 %.

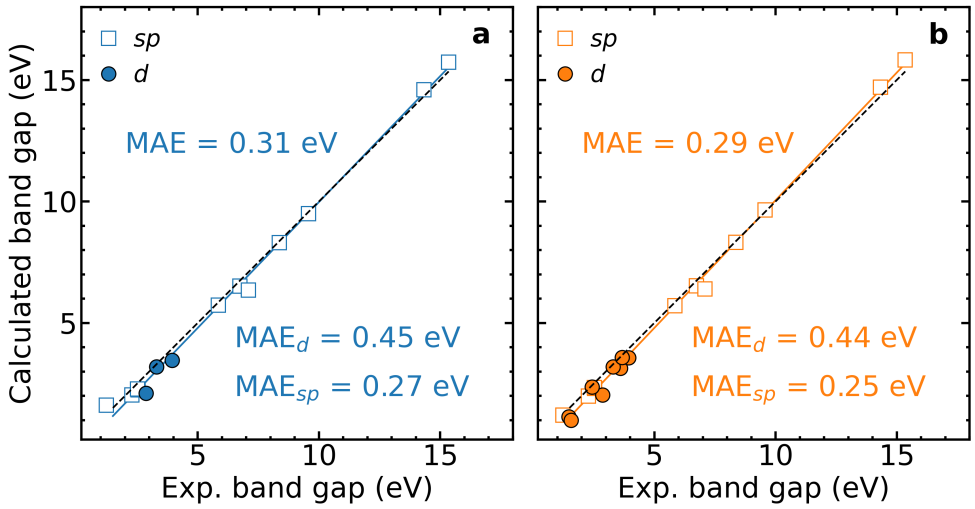

Figure 2: Comparison between the calculated PBE0(α_K) and the ZPR-corrected experimental band gaps through enforcing Koopmans' condition of (a) hydrogen interstitial $H_i(+/0)$ and (b) the potential probe X(+/0) from full self-consistent calculations. Simple *sp* semiconductors are shown with square markers whereas materials with *d* valence electrons are shown with circle markers. For the sake of comparison, materials in Table 1 for which the hydrogen interstitial method does not work are excluded in calculating the MAEs.

We also compare the K-PBE0 results with the quasiparticle self-consistent GW calculations[44,45] with state-of-the-art vertex correction (QSGŴ).[34] The QSGŴ method produces

an overall MAE of 0.11 eV consistently across the table. The MARE increases from 1.9% for *sp* materials to 3.4% and 3*d* semiconductors and we also observe a systematic underestimation of the band gaps of 3*d* materials, which is possibly due to the high *d*-orbital energy error in GW method.[46,47]

With the accuracy of the K-PBE0 functional established, now we turn to the perturbative one-shot approach to simplify the calculation scheme. The approach is based on the follows: for a well-localized defect state, as the ones achieved with the optimized potential probe, the defect wave function calculated at the PBE0 level does not change much from the one calculated at the semilocal PBE level.[48] This allows one to calculate single-particle eigenvalues from the semilocal PBE functionals and avoid the burdensome process of obtaining PBE0 wave functions in a self-consistent manner where the exact exchange needs to be calculated at each step. In other words, we calculate the defect single-particle level as

$$\epsilon_D^{KS} \approx < \psi_D^{PBE} | \hat{\mathbf{H}}_{KS}[\psi_i^{PBE}] | \psi_D^{PBE} > \tag{4}$$

where $\hat{\mathbf{H}}_{KS}[\psi_i^{PBE}]$ represents the full Kohn-Sham Hamiltonian with Fock exchange calculated with the PBE wave functions.

In Figure 3, we show the difference and relative errors in the predicted band gaps obtained with the full self-consistent hybrid calculations and with the one-shot method. We observe that for all the materials considered here, the discrepancies are either less than 0.25 eV, or 5% of the materials band gap, as indicated by the grey bands in Figure 3. The one-shot method produces a MEA of 0.29 eV (see Table S1 in Supporting Information) as compared to 0.30 eV for the full calculation (Table 1), indicating that the fluctuations in α_K brought about by the approximation does not harm the overall accuracy of the Koopmans' scheme with significant reduction in the computational cost. While the standard hybrid calculations commonly take five to ten steps to reach self-consistency, the one-shot method only requires calculating the exact exchange Fock operator once in calculating $\hat{\mathbf{H}}_{KS}[\psi_i^{PBE}]$. By comparing

Table 1: Band gaps (in eV) and obtained α_K using hydrogen interstitial defect and potential probe compared with QSGŴ and experimental values. Zero-phonon renormalizaton (ZPR) corrected experimental band gaps are taken from ref 12 and used as references for calculating the mean error (ME), mean absolute error (MAE) and mean absolute relatively error (MARE). QSGŴ are taken from ref 34. For the validity of comparison, MAEs on the same row only include materials for which data from both methods are available. Since the hydrogen interstitial method is only valid for three $3d$ materials, it is excluded from the $3d$ and total ME, MAE, MARE comparison.

	H(0/+)	X(0/+)			
	$E_g(\alpha_K)$	σ (bohr)	$E_g(\alpha_K)$	QSGŴ	Expt + ZPR
sp semiconductors					
AlAs	2.03(0.12)	0.92	1.99(0.11)	2.39	2.28
AlP	2.25(0.13)	0.20	2.31(0.14)	2.56	2.54
Ar	14.60(0.60)	0.53	14.70(0.61)	14.23	14.33
BN	6.52(0.24)	0.05	6.53(0.24)	6.59	6.74
C	5.73(0.21)	0.14	5.71(0.21)	5.83	5.85
CaO	6.35(0.28)	0.15	6.40(0.29)	6.79	7.09
LiCl	9.50(0.35)	0.31	9.65(0.37)	9.87	9.57
LiF	15.73(0.52)	0.18	15.83(0.53)	15.52	15.35
MgO	8.31(0.34)	0.05	8.32(0.34)	8.37	8.36
Si	—	1.23	1.21(0.14)	1.27	1.23
SiC	2.28(0.15)	0.05	2.34(0.16)	2.56	2.52
ME	−0.13		−0.08	0.01	
MAE	0.26		0.27	0.12	
MARE	5.3%		5.1%	1.9%	
$3d$ materials					
GaN	—	0.29	3.58(0.22)	3.61	3.67
GaP	—	0.86	2.36(0.14)	2.41	2.43
GaAs	—	0.67	1.00(0.09)	1.58	1.57
InP	—	0.78	1.13(0.09)	1.42	1.47
ZnO	—	0.25	3.13(0.25)	3.41	3.60
ZnS	3.46(0.18)	0.30	3.57(0.20)	3.63	3.94
ZnSe	2.11(0.15)	0.07	2.03(0.14)	2.75	2.87
TiO_2	3.19(0.14)	0.05	3.19(0.14)		3.30
ME			-0.39	-0.11	
MAE			0.39	0.11	
MARE			16.6%	3.4%	
ME			-0.20	-0.03	
MAE			0.30	0.11	
MARE			9.4%	2.6%	

the wall time for obtaining ϵ_D^{KS}, we found an average of 85% reduction in computational time in obtaining α_K for the K-PBE0 calculations.

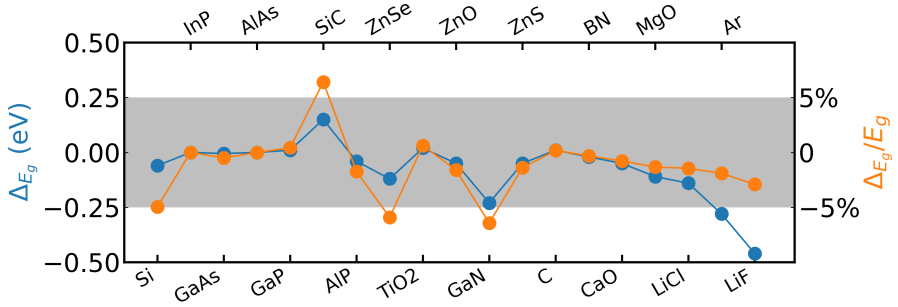

Figure 3: Differences and relative errors in band gap values between the full self-consistent and perturbative one-shot calculations.

To further explore the influence of functional form, we compared the K-PBE0 functional with a Koopmans-compliant CAM functional (K-CAM). The K-CAM functional is designed as follows. The screening parameter μ is set to 0.106 Bohr^{-1} as in HSE06 and α_l is set to $1/\epsilon_\infty$. The latter setting describes correctly the long-range dielectric screening[49–51] and has been shown to produce accurate electronic structures for solid state systems,[12,20,52,52,53] also commonly named as dielectric-dependent hybrid (DDH) functionals. α_s is sought by enforcing Koopmans' condition on the optimized probe state following the same scheme as the K-PBE0 functional we have described so far and annotated as $\alpha_{s,K}$. Details on the resulted $\alpha_{s,K}$, α_l, and band gaps for each material are listed in Table S2 of Supporting Information along with HSE06 results.

In Figure 4, we compare the band gap errors of the K-PBE0 and K-CAM functionals referenced to ZPR-corrected experimental values. We observe that, for simple *sp* materials, the K-CAM functional performs similarly as K-PBE0, producing a MAE of 0.23 eV as compared to 0.25 eV for K-PBE0. The performance is slightly worse for 3*d* materials. The K-CAM functional appears to give a systematic underestimation of the band gaps, especially for Zn-based materials. The MAE increases to 0.53 eV from 0.39 eV of the K-PBE0 functional. These results lead us to the conclusion that, while tuning the range-separated functional by enforcing Koopmans' condition improves the band gap prediction from HSE06 functional

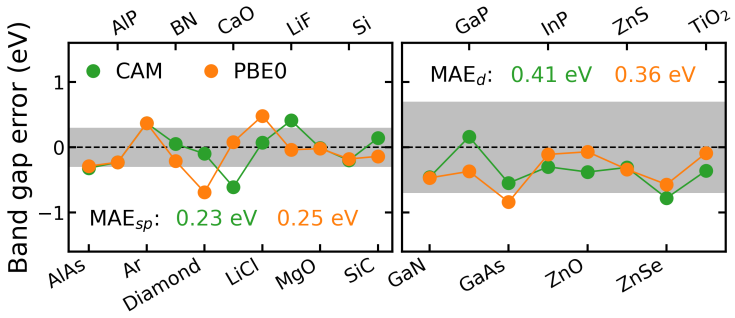

Figure 4: Band gap errors calculated with the CAM($\alpha_{s,K}$,$\alpha_l = 1/\epsilon_\infty$,$\mu_{HSE}$) functional compared to PBE0(α_K). Simple *sp* semiconductors are shown on the left panel whereas materials with *d* valence electrons are shown on the right. The grey bands respective MAEs calculated with CAM functional.

(the total MAE decreases from 1.01 eV to 0.36 eV), the gain in accuracy is minimal, if at all, compared to the K-PBE0 functional. This finding is in agreement with previous works where the tests were done on a smaller set of materials.[17,19]

In summary, we have studied hybrid functional tuning by enforcing Koopmans' condition on defect probe state for an extended list of semiconductors and insulators. We show that while the natural hydrogen interstitial states are heavily delocalized in some materials and render the Koopmans' scheme invalid, the optimized probe works universally across different materials and produces a total MAE of 0.30 eV in band gap with the PBE0(α_K) functional. Out of these values, the accuracy is on average 0.25 eV for simple *sp* materials, and 0.39 eV for 3*d* materials, indicating that the inclusion of *d* orbitals deteriorates the predictions. Based on the rationale that the wave functions of localized defect states do not vary significantly with α, we implemented a perturbative one-shot method in which the PBE wave functions are used to calculate the single-particle PBE0 Hamiltonian and to obtain the eigenvalues. The one-shot method reduces the computation time by 85% comparing to the full self-consistent calculation without undermining the accuracy. Last, we compared the PBE0(α_K) functional with a range-separated CAM functional in which α_l is fixed to $1/\epsilon$, screening parameter 0.106 Bohr^{-1} as in HSE06, and α_s sought by enforcing Koopmans' condition. We find that while this K-CAM functional performs better than HSE06 in terms of averaged accuracy (0.31 eV for the former, 1.01 eV for the latter), the improvement is minimal comparing to

K-PBE0. On account of these findings, we propose the perturbative one-shot approximation with optimized potential probe as a cheap and robust technique for tuning nonempirical hybrid functionals.

Acknowledgement

This work is supported by the Swiss National Science Foundation (SNSF) under Grant No. 200020-152799. We acknowledge computational resources frat Swiss National Supercomputing Center (CSCS) under project s1122 and SCITAS-EPFL.

Supporting Information Available

- Charge transition levels with varying probe width σ (Figure S1); single-particle energy levels in Si with varying α for the hydrogen interstitial and probe (Figure S2); list of band gaps and α_K obtained with the one-shot method (Table S1); list of band gaps and α_K obtained with the CAM functional (Table S2).

References

(1) Hohenberg, P.; Kohn, W. Inhomogeneous Electron Gas. *Phys. Rev.* **1964**, *136*, B864–B871.

(2) Kohn, W.; Sham, L. J. Self-Consistent Equations Including Exchange and Correlation Effects. *Phys. Rev.* **1965**, *140*, A1133–A1138.

(3) Sham, L. J.; Schlüter, M. Density-Functional Theory of the Energy Gap. *Phys. Rev. Lett.* **1983**, *51*, 1888–1891.

(4) Perdew, J. P.; Zunger, A. Self-interaction correction to density-functional approximations for many-electron systems. *Phys. Rev. B* **1981**, *23*, 5048–5079.

(5) Becke, A. D. A new mixing of Hartree–Fock and local density-functional theories. *The Journal of Chemical Physics* **1993**, *98*, 1372–1377.

(6) Perdew, J. P.; Ernzerhof, M.; Burke, K. Rationale for mixing exact exchange with density functional approximations. *The Journal of Chemical Physics* **1996**, *105*, 9982–9985.

(7) Burke, K.; Ernzerhof, M.; Perdew, J. P. The adiabatic connection method: a non-empirical hybrid. *Chemical Physics Letters* **1997**, *265*, 115–120.

(8) Yanai, T.; Tew, D. P.; Handy, N. C. A new hybrid exchange–correlation functional using the Coulomb-attenuating method (CAM-B3LYP). *Chemical Physics Letters* **2004**, *393*, 51–57.

(9) Heyd, J.; Scuseria, G. E.; Ernzerhof, M. Hybrid functionals based on a screened Coulomb potential. *The Journal of Chemical Physics* **2003**, *118*, 8207–8215.

(10) Heyd, J.; Scuseria, G. E.; Ernzerhof, M. Erratum: "Hybrid functionals based on a screened Coulomb potential" [J. Chem. Phys. 118, 8207 (2003)]. *The Journal of Chemical Physics* **2006**, *124*, 219906.

(11) Marques, M. A. L.; Vidal, J.; Oliveira, M. J. T.; Reining, L.; Botti, S. Density-based mixing parameter for hybrid functionals. *Phys. Rev. B* **2011**, *83*, 035119.

(12) Chen, W.; Miceli, G.; Rignanese, G.-M.; Pasquarello, A. Nonempirical dielectric-dependent hybrid functional with range separation for semiconductors and insulators. *Phys. Rev. Materials* **2018**, *2*, 073803.

(13) Alkauskas, A.; Broqvist, P.; Pasquarello, A. Defect levels through hybrid density functionals: Insights and applications. *physica status solidi (b)* **2011**, *248*, 775–789.

(14) Skone, J. H.; Govoni, M.; Galli, G. Self-consistent hybrid functional for condensed systems. *Phys. Rev. B* **2014**, *89*, 195112.

(15) Perdew, J. P.; Parr, R. G.; Levy, M.; Balduz, J. L. Density-Functional Theory for Fractional Particle Number: Derivative Discontinuities of the Energy. *Phys. Rev. Lett.* **1982**, *49*, 1691–1694.

(16) Janak, J. F. Proof that $\frac{\partial E}{\partial n_i} = \epsilon$ in density-functional theory. *Phys. Rev. B* **1978**, *18*, 7165–7168.

(17) Miceli, G.; Chen, W.; Reshetnyak, I.; Pasquarello, A. Nonempirical hybrid functionals for band gaps and polaronic distortions in solids. *Phys. Rev. B* **2018**, *97*, 121112.

(18) Bischoff, T.; Reshetnyak, I.; Pasquarello, A. Adjustable potential probes for band-gap predictions of extended systems through nonempirical hybrid functionals. *Phys. Rev. B* **2019**, *99*, 201114.

(19) Bischoff, T.; Wiktor, J.; Chen, W.; Pasquarello, A. Nonempirical hybrid functionals for band gaps of inorganic metal-halide perovskites. *Phys. Rev. Materials* **2019**, *3*, 123802.

(20) Das, T.; Di Liberto, G.; Tosoni, S.; Pacchioni, G. Band Gap of 3D Metal Oxides and Quasi-2D Materials from Hybrid Density Functional Theory: Are Dielectric-Dependent

Functionals Superior? *Journal of Chemical Theory and Computation* **2019**, *15*, 6294–6312, PMID: 31614082.

(21) Cipriano, L. A.; Di Liberto, G.; Tosoni, S.; Pacchioni, G. Band Gap in Magnetic Insulators from a Charge Transition Level Approach. *Journal of Chemical Theory and Computation* **2020**, *16*, 3786–3798.

(22) Weng, M.; Pan, F.; Wang, L.-W. Wannier–Koopmans method calculations for transition metal oxide band gaps. *npj Computational Materials* **2020**, *6*, 33.

(23) Wing, D.; Ohad, G.; Haber, J. B.; Filip, M. R.; Gant, S. E.; Neaton, J. B.; Kronik, L. Band gaps of crystalline solids from Wannier-localization–based optimal tuning of a screened range-separated hybrid functional. *Proceedings of the National Academy of Sciences* **2021**, *118*.

(24) Kronik, L.; Stein, T.; Refaely-Abramson, S.; Baer, R. Excitation Gaps of Finite-Sized Systems from Optimally Tuned Range-Separated Hybrid Functionals. *Journal of Chemical Theory and Computation* **2012**, *8*, 1515–1531, PMID: 26593646.

(25) Refaely-Abramson, S.; Sharifzadeh, S.; Govind, N.; Autschbach, J.; Neaton, J. B.; Baer, R.; Kronik, L. Quasiparticle Spectra from a Nonempirical Optimally Tuned Range-Separated Hybrid Density Functional. *Phys. Rev. Lett.* **2012**, *109*, 226405.

(26) Borghi, G.; Ferretti, A.; Nguyen, N. L.; Dabo, I.; Marzari, N. Koopmans-compliant functionals and their performance against reference molecular data. *Phys. Rev. B* **2014**, *90*, 075135.

(27) Autschbach, J.; Srebro, M. Delocalization Error and "Functional Tuning" in Kohn–Sham Calculations of Molecular Properties. *Accounts of Chemical Research* **2014**, *47*, 2592–2602, PMID: 24968277.

(28) Colonna, N.; Nguyen, N. L.; Ferretti, A.; Marzari, N. Koopmans-Compliant Functionals and Potentials and Their Application to the GW100 Test Set. *Journal of Chemical Theory and Computation* **2019**, *15*, 1905–1914, PMID: 30640457.

(29) Ju, C.-W.; French, E. J.; Geva, N.; Kohn, A. W.; Lin, Z. Stacked Ensemble Machine Learning for Range-Separation Parameters. *The Journal of Physical Chemistry Letters* **2021**, *12*, 9516–9524, PMID: 34559964.

(30) Hedin, L. New Method for Calculating the One-Particle Green's Function with Application to the Electron-Gas Problem. *Phys. Rev.* **1965**, *139*, A796–A823.

(31) Hybertsen, M. S.; Louie, S. G. Electron correlation in semiconductors and insulators: Band gaps and quasiparticle energies. *Phys. Rev. B* **1986**, *34*, 5390–5413.

(32) Shishkin, M.; Marsman, M.; Kresse, G. Accurate Quasiparticle Spectra from Self-Consistent GW Calculations with Vertex Corrections. *Phys. Rev. Lett.* **2007**, *99*, 246403.

(33) Chen, W.; Pasquarello, A. Accurate band gaps of extended systems via efficient vertex corrections in *GW*. *Phys. Rev. B* **2015**, *92*, 041115.

(34) Tal, A.; Chen, W.; Pasquarello, A. Vertex function compliant with the Ward identity for quasiparticle self-consistent calculations beyond *GW*. *Phys. Rev. B* **2021**, *103*, L161104.

(35) Giannozzi, P. et al. QUANTUM ESPRESSO: a modular and open-source software project for quantum simulations of materials. *Journal of Physics: Condensed Matter* **2009**, *21*, 395502 (19pp).

(36) Giannozzi, P. et al. Advanced capabilities for materials modelling with QUANTUM ESPRESSO. *Journal of Physics: Condensed Matter* **2017**, *29*, 465901.

(37) Giannozzi, P.; Baseggio, O.; Bonfà, P.; Brunato, D.; Car, R.; Carnimeo, I.; Cavazzoni, C.; de Gironcoli, S.; Delugas, P.; Ferrari Ruffino, F.; Ferretti, A.; Marzari, N.; Timrov, I.; Urru, A.; Baroni, S. Quantum ESPRESSO toward the exascale. *The Journal of Chemical Physics* **2020**, *152*, 154105.

(38) van Setten, M.; Giantomassi, M.; Bousquet, E.; Verstraete, M.; Hamann, D.; Gonze, X.; Rignanese, G.-M. The PseudoDojo: Training and grading a 85 element optimized norm-conserving pseudopotential table. *Computer Physics Communications* **2018**, *226*, 39–54.

(39) Hamann, D. R. Optimized norm-conserving Vanderbilt pseudopotentials. *Phys. Rev. B* **2013**, *88*, 085117.

(40) Chen, W.; Pasquarello, A. Correspondence of defect energy levels in hybrid density functional theory and many-body perturbation theory. *Phys. Rev. B* **2013**, *88*, 115104.

(41) Freysoldt, C.; Neugebauer, J.; Van de Walle, C. G. Fully Ab Initio Finite-Size Corrections for Charged-Defect Supercell Calculations. *Phys. Rev. Lett.* **2009**, *102*, 016402.

(42) Tal, A.; Chen, W.; Pasquarello, A. Vertex function compliant with the Ward identity for quasiparticle self-consistent calculations beyond GW. *Materials Cloud Archive* **2020**, *140*.

(43) Cardona, M.; Thewalt, M. L. W. Isotope effects on the optical spectra of semiconductors. *Rev. Mod. Phys.* **2005**, *77*, 1173–1224.

(44) Faleev, S. V.; van Schilfgaarde, M.; Kotani, T. All-Electron Self-Consistent *GW* Approximation: Application to Si, MnO, and NiO. *Phys. Rev. Lett.* **2004**, *93*, 126406.

(45) van Schilfgaarde, M.; Kotani, T.; Faleev, S. Quasiparticle Self-Consistent *GW* Theory. *Phys. Rev. Lett.* **2006**, *96*, 226402.

(46) Jiang, H.; Gomez-Abal, R. I.; Rinke, P.; Scheffler, M. First-principles modeling of localized d states with the GW@LDA + U approach. *Phys. Rev. B* **2010**, *82*, 045108.

(47) Lany, S. Band-structure calculations for the 3d transition metal oxides in GW. *Phys. Rev. B* **2013**, *87*, 085112.

(48) Alkauskas, A.; Pasquarello, A. Effect of improved band-gap description in density functional theory on defect energy levels in α-quartz. *Physica B: Condensed Matter* **2007**, *401-402*, 670–673.

(49) Shimazaki, T.; Asai, Y. Band structure calculations based on screened Fock exchange method. *Chemical Physics Letters* **2008**, *466*, 91–94.

(50) Shimazaki, T.; Asai, Y. First principles band structure calculations based on self-consistent screened Hartree–Fock exchange potential. *The Journal of Chemical Physics* **2009**, *130*, 164702.

(51) Shimazaki, T.; Asai, Y. Energy band structure calculations based on screened Hartree–Fock exchange method: Si, AlP, AlAs, GaP, and GaAs. *The Journal of Chemical Physics* **2010**, *132*, 224105.

(52) Skone, J. H.; Govoni, M.; Galli, G. Nonempirical range-separated hybrid functionals for solids and molecules. *Phys. Rev. B* **2016**, *93*, 235106.

(53) Cui, Z.-H.; Wang, Y.-C.; Zhang, M.-Y.; Xu, X.; Jiang, H. Doubly Screened Hybrid Functional: An Accurate First-Principles Approach for Both Narrow- and Wide-Gap Semiconductors. *The Journal of Physical Chemistry Letters* **2018**, *9*, 2338–2345, PMID: 29669414.

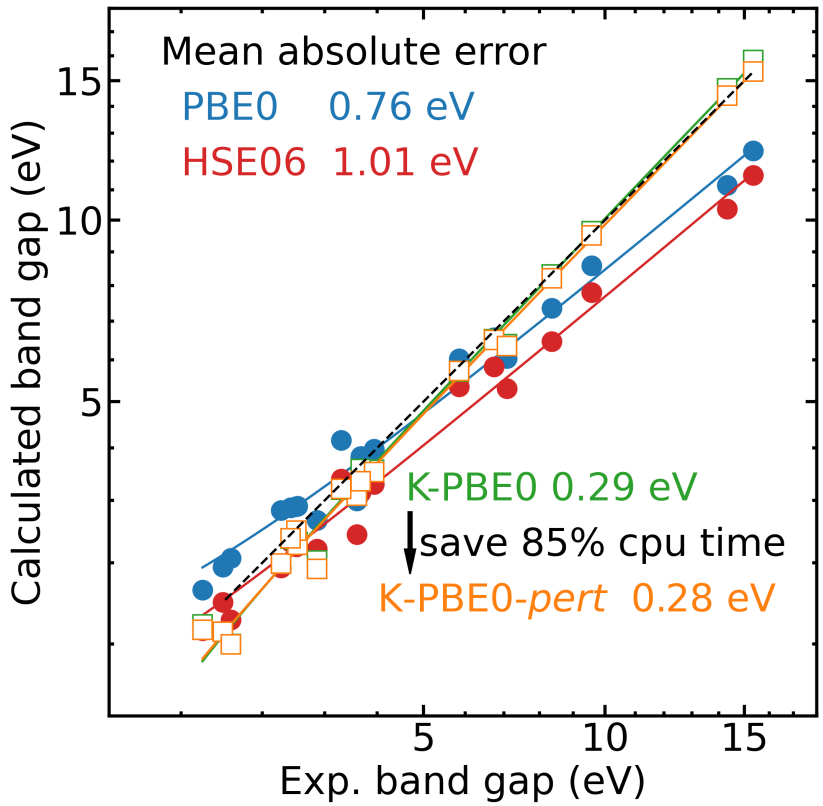

Figure 5: TOC image.